Dynamics and thermodynamics of a nonlinear model for DNA denaturation

Thierry Dauxois* and Michel Peyrard*
Physique Non Linéaire: Ondes et Structures Cohérentes, Faculté des Sciences, 6 Boulevard Gabriel, 21000 Dijon, France and Theoretical Division and Center for Nonlinear Studies, Los Alamos National Laboratory, Los Alamos, New Mexico 87545

A. R. Bishop
Theoretical Division and Center for Nonlinear Studies, Los Alamos National Laboratory, Los Alamos, New Mexico 87545
(Received 15 July 1992)

We present a model for the dynamical structure of DNA that can be considered as an extension of the usual Ising-like statistical approach to the melting curves. The model uses the stretching of the hydrogen bonds in a base pair as its main variable. Numerical simulations at constrained temperature show that it provides a good qualitative description of the collective motions of the base pairs, including their large-amplitude fluctuational openings and the emergence of the denaturation bubbles from the thermal fluctuations. The results are in good agreement with a statistical-mechanics analysis of the denaturation and specific-heat curves, performed with the transfer-integral method, provided that discreteness effects are treated exactly by a numerical solution of the transfer-integral operator. Second-order self-consistent phonon theory agrees with the exact transfer-integral results in the low- and intermediate-temperature ranges and explains the phonon softening observed in the molecular-dynamics simulations. When the temperature approaches the denaturation temperature, the second-order self-consistent phonon results deviate significantly from the exact ones, pointing to the fundamental role of nonlinear processes in DNA denaturation.

PACS number(s): 87.10.+e, 63.70.+h, 64.70.−p

I. INTRODUCTION

The discovery of DNA structure has highlighted the fundamental relationship between structure and function in molecular biology. This connection is now well established and even used every day by drug companies looking for new active molecules. However, there is now a growing feeling that *static* structure alone does not entirely determine the biological function of a molecule. Molecular dynamics has perhaps been at the origin of this attitude [1] because it has shown that chemical reactions that seem to be impossible according to the molecular structure might indeed take place due to temporary large molecular distortions.

DNA transcription is a typical example in which the dynamics of the molecule is essential to a biological function since the double helix has to be locally opened in order to expose the coding bases to chemical reactions. This process is, however, very complex because it is activated by an enzyme and it is probably still beyond a detailed analysis. Thermal denaturation has some similarities with the transcription because it starts locally by the formation of a so-called "denaturation bubble" similar to the local opening occurring in the transcription. Therefore investigating thermal denaturation is a valid preliminary step toward the understanding of the transcription. At temperatures well below the denaturation temperature, DNA also shows large-amplitude motions known as "fluctuational openings" in which base pairs open for a very short time and then close again. These motions are important because, when the base pairs reclose, they can trap some external molecules causing a defect in the sequence. This process has been proposed as a possible mechanism of chemical carcinogenesis [2]. The fluctuational openings can be considered as intrinsic precursors to the denaturation.

The denaturation or "melting" transition is the separation of the two complementary strands. It can be induced by heating or by changing the ionicity of the solvent. It has been extensively investigated experimentally and models have been proposed to explain the complicated denaturation curves found in the experiments [3]. However, these models are essentially Ising-like where a base pair is considered as a two-state system which is either closed or open. Such an approach cannot reproduce the full dynamics of the denaturation and it relies on phenomenological parameters for the probability of opening or cooperative character of this opening, which are not easily derivable from first-principles calculations.

On the other hand, the nonlinear lattice dynamics of DNA has recently been the subject of many investigations based on the idea that vibrational energy might be trapped into solitary-wave excitations. This idea, originally suggested by Englander *et al.* [4] to explain the open states of the DNA molecule, has given rise to many investigations using solitonlike solutions to describe open states, transition between the *A* and *B* forms, or energy transport along the molecule [5-8]. Most of these investigations have focused on the *propagation* of solitons along the double helix. However, the biological function of DNA does not necessarily involve transport along the molecule. Consequently, although it is clear that a realistic model will exhibit nonlinear effects owing to the very large amplitude motions known to exist, their ability to

propagate along the helix is not a requirement of the model. Rather, for denaturation (and transcription) we are concerned by the *formation and growth* of these excitations. It is the question that we want to investigate in this paper. This is an extension to nonlinear dynamics of the Ising models mentioned above. As in the Ising models, however our approach uses a very simple description of the molecule restricted to the most relevant degrees of freedom.

The model was introduced in a previous work [9] in which we investigated its statistical mechanics and determined its denaturation temperature in a continuum limit. An analysis in terms of a nonlinear Schrödinger (NLS) equation for medium-amplitude excitations suggested that the denaturation could be achieved through an energy localization process leading to the formation of large-amplitude nonlinear excitations. In the present paper we study the nonlinear dynamics of the model in contact with a thermal bath and we analyze its evolution as temperature approaches the melting point. We show that, while it is dominated by extended waves (phonons) interacting nonlinearly at low temperature, the role of localized excitations grows as temperature rises. These excitations are responsible for the melting. Section II introduces the model and exact statistical-mechanics results deduced from the transfer-integral approach which show that it does show a thermal denaturation. Section III investigates the mechanism of this denaturation through molecular-dynamics simulations at constrained temperature. Finally, in Sec. IV a self-consistent phonon theory is used to discuss some of these results, to provide an analysis of the melting process, and to derive analytical expressions of some thermodynamical functions in the low- and high-temperature regimes.

II. MODEL AND TRANSFER OPERATOR APPROACH

Previous attempts to model the thermal denaturation of DNA used Ising models[3] in which a base pair was treated as a two-state system being either closed or open. Here we want to go further but still keep the model as simple as possible in an attempt to determine the fundamental mechanism of the melting. Therefore we consider a simplified geometry for the DNA chain in which we neglect the asymmetry of the molecule and we represent each strand by a set of point masses which correspond to the nucleotides. The main characteristics of the model are as follows.

(i) The longitudinal displacements are not considered because their typical amplitudes are significantly smaller than the amplitudes of the smaller transverse ones [10]. The displacements from equilibrium of the nth nucleotide are denoted w_n for one chain and v_n for the other.

(ii) Two neighboring nucleotides of the same strand are connected by a harmonic potential to keep the model as simple as possible. On the other hand, the bonds connecting the two bases belonging to different strands are extremely stretched when the double helix opens locally so that their nonlinearity must not be ignored. We use a Morse potential to represent the transverse interaction of the bases in a pair. It describes not only the hydrogen bonds but the repulsive interactions of the phosphate groups, partly screened by the surrounding solvent action as well.

The Hamiltonian for the model is then

$$H=\sum_n \left[\frac{1}{2}m(\dot{w}_n^2+\dot{v}_n^2)+\frac{K}{2}[(w_n-w_{n-1})^2+(v_n-v_{n-1})^2] + D(e^{-a(w_n-v_n)/\sqrt{2}}-1)^2 \right] . \quad (1)$$

We can obtain a more convenient form by introducing variables that would correspond to normal coordinates in the linear limit, $x_n=(w_n+v_n)/\sqrt{2}$ and $y_n=(w_n-v_n)/\sqrt{2}$, yielding

$$H=\sum_n \left[\frac{1}{2}m\dot{x}_n^2+\frac{K}{2}(x_n-x_{n-1})^2 \right] + \left[\frac{1}{2}m\dot{y}_n^2+\frac{K}{2}(y_n-y_{n-1})^2+D(e^{-ay_n}-1)^2 \right] . \quad (2)$$

The part of the Hamiltonian that depends on the variable x_n is decoupled from the stretching part and corresponds merely to a harmonic chain without substrate potential. It is well behaved so that we can ignore this term in the statistical mechanics of the model. Therefore we henceforth consider only the part of H which depends on y_n,

$$H_y=\left[\frac{1}{2}m\dot{y}_n^2+\frac{K}{2}(y_n-y_{n-1})^2+D(e^{-ay_n}-1)^2 \right] \quad (3)$$

and describes the dynamics of the stretching motions we are interested in.

Since we are interested in the thermal denaturation transition of the molecule, the natural approach is to investigate the statistical mechanics of the model. Because of the one-dimensional character of the system, and because the interactions are restricted to nearest-neighbor interactions, it can be treated exactly, including fully the nonlinearities, with the transfer-operator method.[9]

For a chain containing N units with periodic boundary conditions, the classical partition function, given in terms of the Hamiltonian (3), may be factored as

$$Z=\int_{-\infty}^{+\infty}\prod_{n=1}^{N} dy_n dp_n e^{-\beta H_y}\delta(p_1-p_N)\delta(y_1-y_N) = Z_p Z_y . \quad (4)$$

The momentum part are readily integrated to give the familiar kinetic factor for N particles $Z_p=(2\pi m k_B T)^{N/2}$. Since the coupling involves only nearest-neighbor interactions, Z_y can be expressed in the form

$$Z_y=\int_{-\infty}^{+\infty}\prod_{n=1}^{N} dy_n e^{-\beta f(y_n,y_{n-1})}\delta(y_1-y_N) , \quad (5)$$

where f denotes the potential energy in y_n of the Hamiltonian (2). This integral (5) can be evaluated exactly in the thermodynamic limit of a large system ($N\to\infty$) using the eigenfunctions and eigenvalues of the transfer-

integral operator [11-13]

$$\int dy_{n-1} e^{-\beta f(y_n, y_{n-1})} \phi_i(y_{n-1}) = e^{-\beta \epsilon_i} \phi_i(y_n) \ . \quad (6)$$

The calculation is similar to the one performed by Krumhansl and Schrieffer[12] for the statistical mechanics of the ϕ^4 field. It yields $\mathcal{Z}_y = \exp(-N\beta\epsilon_0)$, where ϵ_0 is the lowest eigenvalue of the operator. We can then compute the free energy of our model as the sum of the different contributions in $\mathcal{Z}$,

$$\mathcal{F} = -k_B T \ln \mathcal{Z} = -\frac{N k_B T}{2} \ln(2\pi m k_B T) + N\epsilon_0 \ . \quad (7)$$

From this result we can derive the specific heat

$$C_v = -T \frac{\partial^2 \mathcal{F}}{\partial T^2} \ . \quad (8)$$

The quantity which gives a measure of the extent of the denaturation of the molecule is the mean stretching $\langle y_m \rangle$ of the hydrogen bonds, which is given by

$$\langle y_m \rangle = \frac{1}{\mathcal{Z}} \int \prod_{n=1}^{N} y_m e^{-\beta H_y} \delta(y_1 - y_N) \delta(p_1 - p_N) dy_n dp_n$$

$$= \frac{1}{\mathcal{Z}_y} \int \prod_{i=1}^{N} y_m e^{-\beta f(y_n, y_{n-1})} \delta(y_1 - y_N) dy_n \ . \quad (9)$$

As the model is assumed to be homogeneous, the result does not depend on the particular site m considered. The integral can again be calculated with the transfer-integral method[11] and yields

$$\langle y \rangle = \langle y_m \rangle = \frac{\sum_{i=1}^{N} \langle \phi_i(y) | y | \phi_i(y) \rangle e^{-N\beta\epsilon_i}}{\sum_{i=1}^{N} \langle \phi_i(y) | \phi_i(y) \rangle e^{-N\beta\epsilon_i}}$$

$$= \langle \phi_0(y) | y | \phi_0(y) \rangle = \int \phi_0^2(y) y \, dy \ , \quad (10)$$

since in the limit of large N, the result is again dominated by the lowest eigenvalue ϵ_0 associated with the normalized eigenfunction $\phi_0(y)$.

In the continuum limit approximation, the transfer-integral eigenvalue problem can be reduced to the following Schrödinger-like equation:

$$-\frac{1}{2\beta^2 K} \frac{\partial^2 \phi_i}{\partial y^2} + D(e^{-2ay} - 2e^{-ay}) \phi_i(y)$$

$$= (\epsilon_i - s_0 - D) \phi_i(y) \ , \quad (11)$$

with $s_0 = (1/2\beta)\ln(\beta K/2\pi)$.

Equation (11) is formally identical to the Schrödinger equation for a particle in a Morse potential, so that it can be solved exactly [14,15]. When

$$T_d = \frac{2\sqrt{2KD}}{a k_B} > T \ , \quad (12)$$

it has a discrete spectrum which corresponds to localized eigenfunctions. On the contrary, above T_d, Eq. (11) has only delocalized states. We can therefore consider T_d as the melting temperature. The expression of the eigenvalue of the ground state is

$$\epsilon_0 = \frac{1}{2\beta} \ln\left[\frac{\beta K}{2\pi}\right] + \frac{a}{\beta}\left[\frac{D}{2K}\right]^{1/2} - \frac{a^2}{8\beta^2 K} \ . \quad (13)$$

However, experiments on proton exchange in DNA [16] show some evidence of exchange limited to a single base pair which suggests that discreteness effects can be extremely large in DNA. Therefore the calculation presented above must be completed by an investigation able to describe this extremely discrete case. The lattice effects in this case go certainly beyond perturbation corrections [17] and therefore we have solved numerically without approximations the eigenvalue equation of the transfer operator [18] by symmetrizing the transfer-integral operator and replacing the integral by sums of discrete increments, using summation formulas at different orders. The problem is then equivalent to finding the eigenvalues and eigenvectors of a symmetric matrix.

Figure 1 compares the thermal evolution of $\langle y_m \rangle$ obtained with the continuum approximation [Eqs. (10) and (11)] and the exact numerical calculation, for the model parameters discussed in the next section. Both methods show a divergence of the hydrogen bond stretching over a given temperature, but the melting temperatures given by the numerical treatment is significantly higher, pointing out the large role of discreteness in DNA dynamics if one uses realistic parameters for the model. The numerical

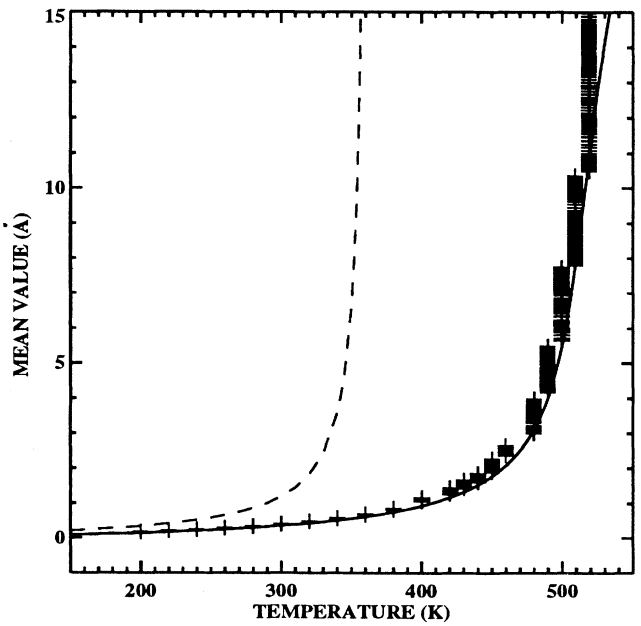

FIG. 1. Variation of $\langle y \rangle$ vs temperature: The solid line corresponds to the exact numerical calculation, the dashed line to the results obtained with the continuum approximation, and the plus signs to molecular-dynamics simulations.

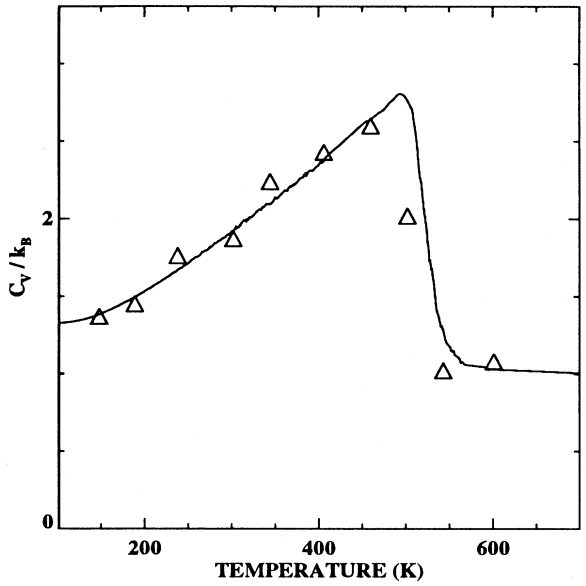

FIG. 2. Variation of the specific heat vs temperature: The solid line corresponds to the transfer-integral results and the symbols correspond to molecular-dynamics simulations.

results for the specific heat versus temperatures given by the transfer-integral calculation are shown in Fig. 2.

III. MOLECULAR-DYNAMICS CALCULATIONS

The thermodynamics of our DNA model shows that it exhibits a thermal evolution which is qualitatively similar to the denaturation of the molecule observed experimentally. But this statistical approach does not give informations on the *mechanism* of the denaturation, and in particular, does it start locally by the formation of denaturation bubbles in agreement with the experiments? In order to study this aspect, we have investigated the dynamics of the model in contact with a thermal bath by molecular-dynamics simulation with the Nose method.

Beginning with the Hamiltonian H_y and the $2N$-dimensional phase space of a chain of N base pairs with periodic boundary conditions, the fixed temperature canonical ensemble can be simulated by the addition of a single variable s, which regulates the energy flows, and an additional parameter M, which fixes the scale of the temperature fluctuations. The augmented Hamiltonian [19,20] is then introduced in the form

$$H'=H_y+\frac{p_s^2}{2M}+(N+1)k_BT\ln s \ , \tag{14}$$

where T denotes the temperature of the system and k_B is the Boltzmann's constant. The logarithmic character of the potential energy of the heat bath is introduced to achieve the equivalence of the canonical ensemble for the original system. Indeed, Nose demonstrated that in this extended phase space the microcanonical ensemble of H' is precisely the canonical ensemble of H_y at temperature T. This property is only exact for equilibrium properties, but investigations currently in progress [21] show that, provided that the characteristic time of the Nose thermostat, controlled by M, is properly chosen, it can also give reliable results for the dynamical properties.

In Hoover's reformulation [22] of Nose's method, the variable s is removed, the equation of motion for s and $\dot{s}$ are replaced by a single equation, and the factor $(N+1)$ is replaced by N. So, defining a thermodynamic friction coefficient $\xi=p_s/M$ and redefining the time interval $dt\rightarrow dt/s$, the Hoover formulation of the equations of motion is

$$m\ddot{y}_n=K(y_{n+1}+y_{n-1}-2y_n) +2aD(e^{-ay_n}-1)e^{-ay_n}-\xi m\dot{y}_n \ , \tag{15}$$

where

$$\dot{\xi}=\frac{1}{M}\left[\sum_n m\dot{y}_n^2-NT\right] .$$

Most of the simulations have been performed with a chain of 256 base pairs with periodic boundary conditions, but in order to achieve better statistics, some simulations have been performed on a Connection Machine-200 with 16 384 base pairs. Equations (15) are integrated with a fourth- order Runge-Kutta scheme with a time step chosen to conserve H' to an accuracy better than 0.001% during a run.

We have chosen a system of units adapted to the energy and time scales of the problem. Energies are expressed in electron volts, masses in atomic mass unit (a.m.u.), and length in angströms. The resulting time unit is 1 t.u. $=1.0214\times10^{-14}$ s. The choice of appropriate model parameters is a very controversial topic, as attested to by the debate in the literature [23]. There are well-established force fields for molecular dynamics of biological molecules, but they have been designed to provide a good description of the *small* amplitude motions of the molecule and are not reliable for the very *large* amplitude motions involved in the denaturation. In our model, the Morse potential is an effective potential which links the two strands. It results from a combination of an attractive part due to the hydrogen bonds between two bases in a pair and the repulsive interaction between the charged phosphate groups on the two strands. The potential for the hydrogen bonds can be rather well estimated [24] but the repulsive part is harder to determine because the repulsion is partly screened by ions of the solvent. Consequently, we have had to rely on estimations. The parameters that we use have been chosen to give realistic properties for the model in terms of vibrational frequencies, size of the open regions, etc., but future work will be needed to confirm our choice. However, we do not expect that a better choice would change *qualitatively* the results presented here. The parameters that we have chosen are a dissociation energy $D=0.04$ eV, a spatial scale factor of the Morse potential $a=4.45$ Å^{-1}, a coupling constant $K=0.06$ eV/Å, and a mass $m=300$ a.m.u. The constant of the Nose thermostat has been set to $M=1000$.

A first scan of the dynamics of the model is obtained by imposing a slow temperature ramp (200–540 K) that generates sets of states which are approximately equili-

brated and are used then as initial states for simulations at constant temperature. Figure 3 shows a summary of the melting process as it appears for a slow heating. In the low-temperature range, patterns of darker regions appear. Moving along the DNA chain (horizontal axis on the figure), one notices that the stretching amplitude exhibits large variations. Dark regions of large stretching are separated by lighter domains where the stretching is small. This is consistent with the fluctuational openings that are observed experimentally [25,26] and means that, even at rather low temperature, this nonlinear system is far from a situation of energy equipartition. When the temperature is higher, the figure shows large black spots which correspond to open regions of the molecule, i.e., the "denaturation bubbles" observed experimentally. They appear as alternatively black and white which shows that they are oscillating. At the highest investigated temperature, the complete chain is black on the figure, which corresponds to the fully denaturated state in which all the base pairs are stretched up to a value which corresponds to the plateau of the Morse potential.

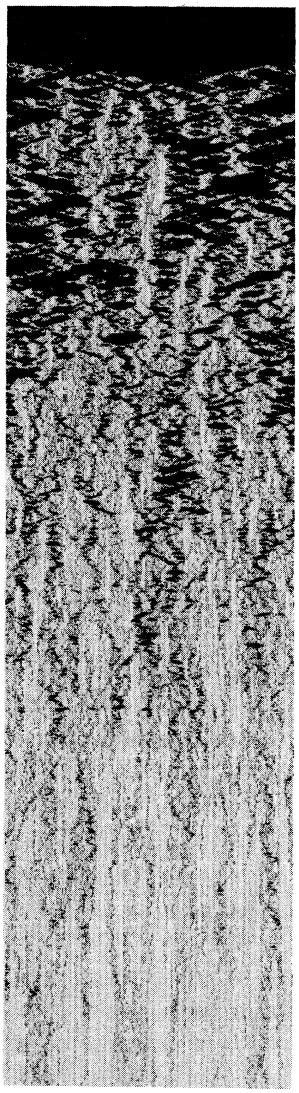

FIG. 3. Evolution of the stretching y along the DNA model during heating. The horizontal axis indicates the position along the 256 cells of the molecule and the vertical axis corresponds to the temperature (or time since t and temperature T are linearly related by the equation of the temperature ramp: $T=T_0+rt$). The temperature increases from 200 K (bottom) to 540 K (top). The grey scale goes from $y \leq 0$ Å (white) to $y \geq 2$ Å (black).

A more accurate picture is obtained by using the Nose scheme correctly, i.e., at constant constrained temperature. The pictures in Fig. 4 show the dynamics at three different temperatures. The dark regions are organized into lines which attest that some excitations are long lived in the system. Following one of these lines, one can notice that it is interrupted regularly and looks like a dotted line. This is due to an *internal breathing* of the localized excitations that oscillate between a large amplitude (black dots in the figure) and a small amplitude state (light dots) in a regular manner. As mentioned in our previous work [9], these results are consistent with the small amplitude expansion of the equation of motion. A multiple scale expansion gives a nonlinear Schrödinger equation, which indeed has breathing solutions. A more careful study [27], with a potential having qualitatively the same profile, has shown that the discreteness of the chain could be of great importance to stabilize the excitations, particularly when breathers are involved. Using an efficient Green's-function method, we obtained a qualitative and quantitative agreement between analytical predictions and simulations.

At $T=150$ K, the excitations are extremely localized (a few units), but if the temperature is raised to $T=340$ K, their sizes grow. Some of them maintain an oscillating motion, whereas others stay in an open state. At $T=450$ K, we see that the picture is dominated by black areas: The system is about to be completely denaturated. We have not yet found an analytical expression of the open bubble—it cannot be represented by the nonlinear Schrödinger equation. An explicit introduction of the thermal fluctuations which are required to stabilize the open states is necessary. The effective potential that we derive in the last section can be viewed as a step in this direction. As the amplitude increases, the frequency of the oscillation decreases to zero, where the bubble stays open. This transition from oscillating to static bubbles is qualitatively similar to a softening of the phonons modes as illustrated by Fig. 5.

The wave-vector-dependent spectral functions, obtained from the molecular-dynamics data, are represented in Fig. 5 for $q=\pi/2$. The solution $y_n(t)$ of the equations of motion were Fourier transformed with respect to both space and time to obtain

$$u(q,\omega)=\sum_i \int_0^{t_{\max}} dt\, u_j(t) e^{i(qj-\omega t)} .$$

The spectral function is then, according to the Wiener-Khinchin theorem,

$$S(q,\omega)=\lim_{t_{\max}\to\infty} \frac{1}{2t_{\max}} \frac{1}{N} |u_{t_{\max}}(q,\omega)|^2 .$$

The spectra shown are obtained after a convolution with a Gaussian in order to smooth the data. The dynamical

structure factor at $T=20$ K shows three features: (i) a well-defined peak around $\omega=0.75$ corresponding to the low-temperature phase phonon peak,

$$\omega^2=\frac{2a^2D+4K\sin^2(q/2)}{m}\ ; \tag{16}$$

(ii) a dc component; and (iii) a first harmonic of the phonon's frequency which show that even at this low temperature the nonlinearity is important. At $T=150$ K, the phonon peak has considerably broadened indicating that the phonon lifetime is shorter and the phonon's frequency has decreased significantly. On the other hand, the central peak has increased, and is now predominant, since it is an order of magnitude larger than the phonon peak. This feature may be due to localized, large-amplitude excitations, similar to breather modes. These modes consist of excitations with an internal oscillation in the phonon's gap, thus they may contribute to the low-frequency dynamical structure factor. As, in our model, there is only one minimum, even local, of the potential, there are no domain walls that could contribute to the central peak. The low-frequency contribution originates from the breathers, in addition to phonon-difference processes. At high temperature ($T=450$ K), a well-defined phonon peak is again present with a small weight at $\omega=0$. The frequency of the peak corresponds to the high-temperature phonon's peak. Recalling that we observed in Fig. 3, that at this temperature most of the particles are on the plateau of the Morse potential, it is clear that this peak results from the phonons on the plateau: $\omega^2=4K/m\sin^2(q/2)$. This is a complete softening, in the sense that the frequency of the lower band

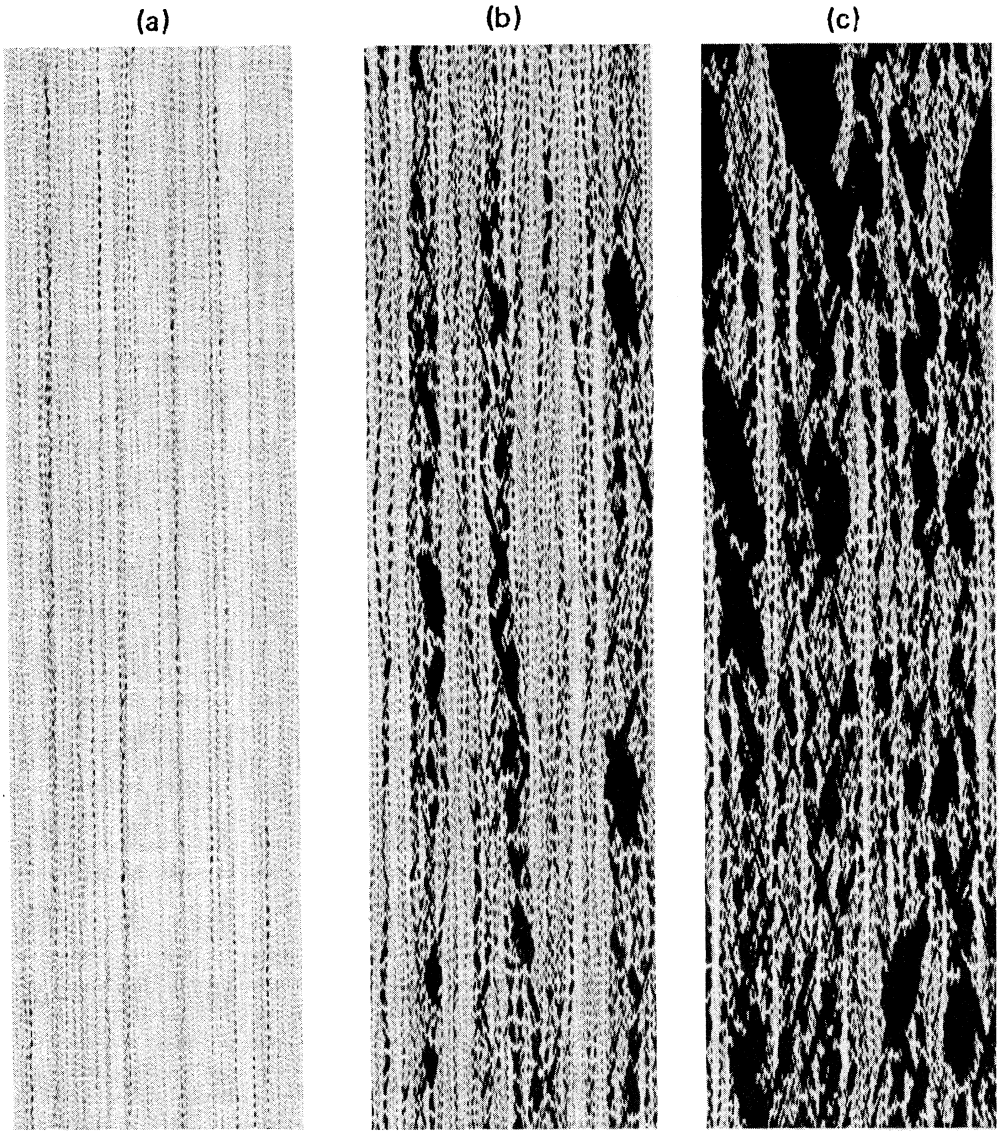

FIG. 4. Evolution vs time of the stretching for three equilibrium temperatures: (a) $T=150$ K, (b) $T=340$ K, (c) $T=450$ K. The grey scale goes from $y\leq -0.1$ Å (white) to $y\geq 1$ Å (black).

edge has reached zero: The potential being flat on the plateau, there is no frequency gap.

In Fig. 6, we plot the frequency of the phonons as a function of the temperature. The errors bars are defined as the width at half-height: They are large at intermediate temperature, but the decrease of the frequency as T increases is clear. The picture shows the evolution, during the transition, of the frequency from its value in the bottom of the well, to the frequency on the Morse plateau. It is a transition from an optical mode to an acoustical one, since on the plateau there is no longer a frequency gap.

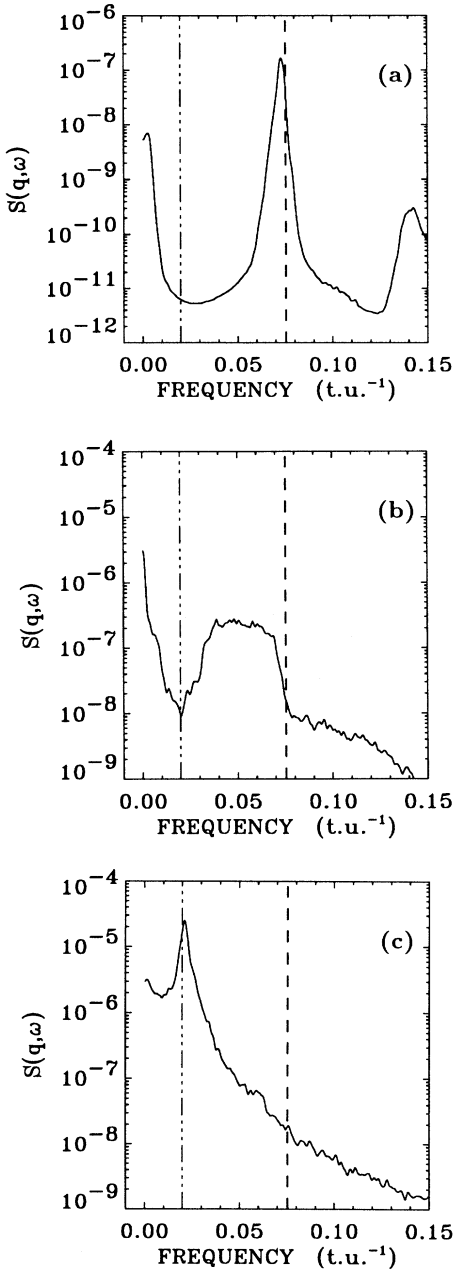

FIG. 5. Dynamical structure factor (semilogarithmic plot) for the stretching y vs the frequency at $q=\pi/2$. (a), (b), and (c) refer to simulations at $T=20$, 150, and 450 K, respectively. The vertical line on the right (dashed) corresponds to the phonon frequency at the bottom of the well, whereas the left one (dash-dot-dot-dot) corresponds to the frequency on the Morse plateau.

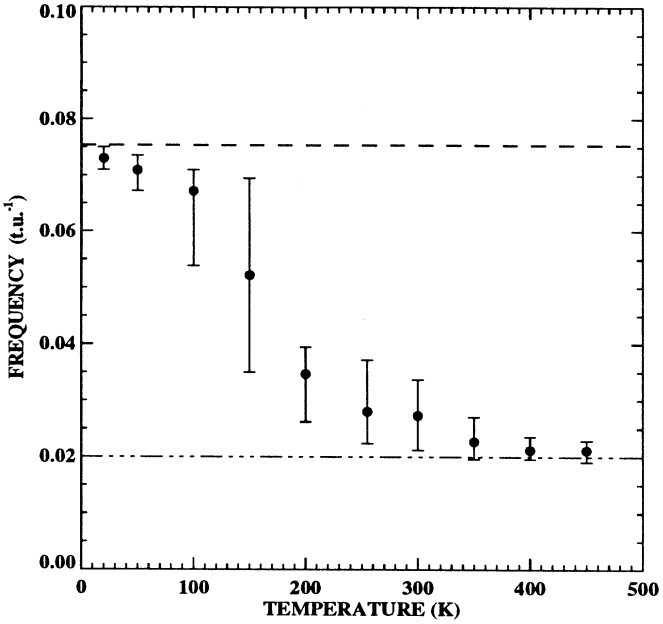

FIG. 6. Frequency of the phonon vs temperature for $q=\pi/2$. The error bars indicate an interval where the frequency lies at those temperatures for which a single mode cannot be identified. The horizontal lines correspond to the phonon frequency at the bottom of the well (dashed) and on the Morse plateau (dash-dot-dot-dot).

The order parameter η of the system, $\langle y \rangle$, is the average displacement, averaged over all sites: $\langle y \rangle = \langle (1/N) \sum_n y_n \rangle$. The molecular-dynamics results for $\langle y \rangle$ are shown in Fig. 1 where they are compared with the value given by the transfer-integral method. In order to obtain better statistics and generate meaningful curves, the simulation has been repeated with 16 384 units on a Connection Machine-200 using one processor for each unit. At very low temperature, η approaches the only stable minimum of the substrate potential $y_s=0$. At high temperature, it rises. When the temperature is high enough, the whole chain is on the Morse plateau, and the system has reached a delocalized state, which we called the denaturated state. In this domain, in spite of the large number of base pairs used in the simulation, the results still show important fluctuations near the transition, since η diverges.

In the biological experiments, in order to study the melting transition of DNA, the separation of the two strands is investigated by monitoring the increase in UV absorbance associated with a change in the electronic configuration of the bases as they unstack, and plotting the fraction of broken base pairs versus temperature. The shape of the melting curve depends strongly of the length of the particular DNA molecule. For short molecules, the denaturation occurs in a highly cooperative manner and is rather sharp. On the contrary for a long molecule, the denaturation can extend over tens of de-

grees and is a multistep process. The numerical results for the denaturation rate are presented in Fig. 7. The importance of using a large number of base pairs is clear from the picture because the noise is still important on some of the curves. The fluctuations at high temperature are caused by the opening or closing of large denaturation bubbles. When comparing these curves with the smooth denaturation curves obtained experimentally, one must keep in mind that the smallest experimental samples contain millions of base pairs. In spite of the simplification of our model and the exceptional computing power of the Connection Machine, this is beyond the present numerical possibilities so that we cannot expect accurate measurements of the denaturation temperature from the simulations. A precise analysis of the state of the chain shows an evolution in qualitative agreement with experimental results. Figure 8 presents the histogram of the width of the bubbles which exceeds a threshold of 0.5 Å, for three different temperatures. We can note two different regimes: At low and intermediate temperatures, there is a quasilinear curve (in semilogarithmic plot), whereas at high temperature, the picture shows a plateau which indicates that there are bubbles at all scales, including very large ones, when the denaturation occurs.

We have obtained an estimate of the transition temperature T_d from the evolution of η, but the specific heat could give us more details on the type of transition. Its value can be obtained from the fluctuations of the kinetic or potential energies in the microcanonical ensemble. The expression is

$$C_v = \left[2 - \frac{4\langle \Delta\phi^2 \rangle}{N(k_B T)^2} \right]^{-1}, \tag{17}$$

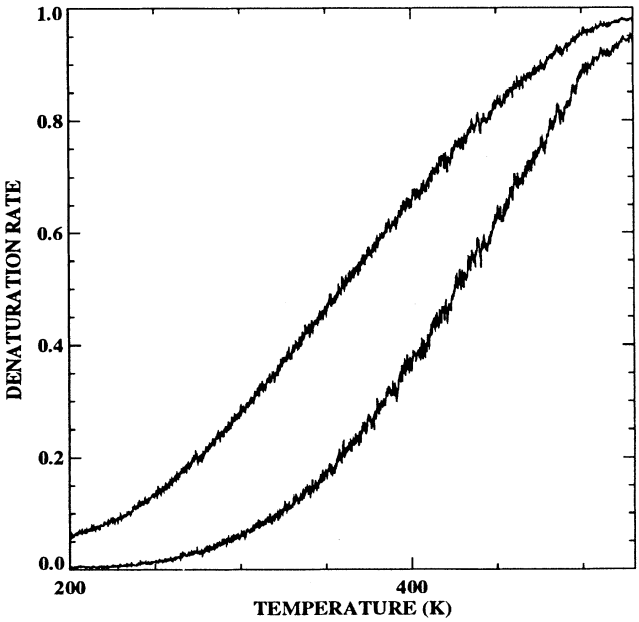

FIG. 7. Denaturation curve for DNA models. The denaturation rate is calculated by counting the number of base pairs which have a mean stretching exceeding a threshold of 0.5 Å (upper curve) and 1 Å (lower curve).

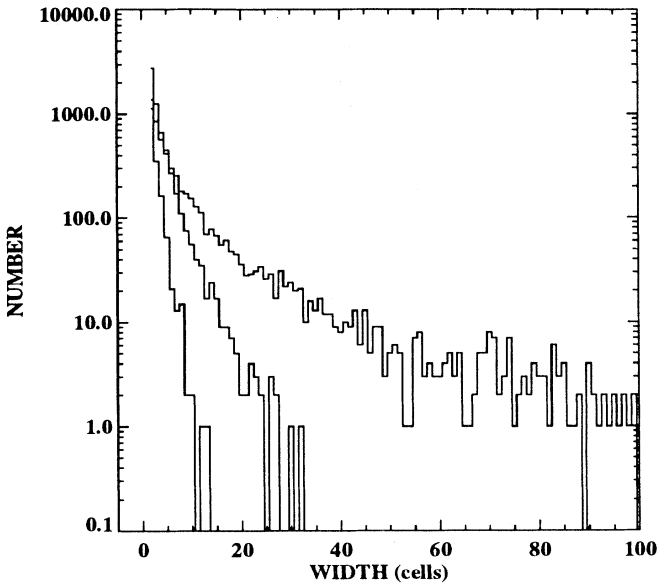

FIG. 8. Histogram of the width (in number of units) of bubbles, with a displacement which exceeds 0.5 Å (semilogarithmic plot). The three curves corresponds to the three following cases: $T=100$, 200, and 450 K. The width of bubbles exceeding 100 units are not plotted.

where $\langle \Delta\phi^2 \rangle$ denotes the average square fluctuations in the total kinetic or potential energies [28]. Notice that, to calculate the specific heat per particle in units of k_B, we have fixed the Nose parameter ξ to zero, in order to run the simulation at constrained energy. The evaluation of a quantity from the mean-square fluctuations is always less accurate than an evaluation using mean values of the quantities themselves. However, the numerical results for C_v show a tendency toward singular behavior which is sufficient to identify a temperature range in which T_d must lie. The equations are integrated for a system of 512 particles, with a time step of 0.25 t.u. With this time step the energy is conserved to within a few part in 10^6. The procedure for each point is as follows. Once a temperature is chosen, the system is aged for 200 000–400 000 time steps to reach thermal equilibrium. Then the equations are integrated during approximately 5 ns, or 2×10^6 times steps, and the data are accumulated every 20 time steps. The specific-heat values are shown in Fig. 2. The broad maximum in the specific heat is near $T=500$ K. We can see that the transition extends over a large temperature region and occurs at a rather high temperature.

IV. SELF-CONSISTENT PHONON METHOD

Because the Schrödinger equation approximation for the transfer-integral operator method breaks down due to the discreteness effects, the transfer-integral approach cannot provide an analytical expression for the thermodynamics quantities like the free energy or the specific heat. Moreover, the molecular-dynamics calculation have exhibited a phonon softening which is important to analyze because it is amenable to experimental observation. Finally, we have noticed on the molecular-

dynamics results the formation of open states which could perhaps be explained within the framework of an effective potential integrating the thermal fluctuations. This is exactly what the self-consistent phonon (SCP) approach calculates. This is why we have applied the SCP method to analyze the properties of our DNA model at thermal equilibrium. We have been able to evaluate explicitly the second-order correction which gives successful results, at least sufficiently far from the transition temperature.

In the low-temperature regime, introducing $u_n = y_n - \langle y \rangle = y_n - \eta$ and two parameters Ω^2 and ϕ, we apply the SCP method [29], by considering the trial harmonic Hamiltonian

$$H_0 = \sum_n \left[\frac{1}{2} m \dot{u}_n^2 + \frac{\phi}{2}(u_n - u_{n+1})^2 + \frac{\Omega^2}{2} u_n^2 \right] . \quad (18)$$

The canonical partition function $\mathcal{Z}$ can be expressed as the product of the unperturbed partition function $\mathcal{Z}_0$ and the perturbation factor $\mathcal{Z}_1$:

$$\begin{aligned} \mathcal{Z} &= \int \prod_i du_i e^{-\beta V} \\ &= \left[\int \prod_i du_i e^{-\beta H_0} \right] \langle e^{-\beta(H - H_0)} \rangle_0 \\ &= \mathcal{Z}_0 \mathcal{Z}_1 . \end{aligned}$$

The perturbation series for $\mathcal{Z}_1$ is calculated by expanding the exponential and the logarithmic function; the coefficient of $(-\beta)^n/n!$ in the expansion of $\ln \mathcal{Z}_1$ is termed the nth cumulant and is written [30] $\langle (H - H_0)^n \rangle_{0,c}$. Thus

$$\begin{aligned} \mathcal{F} &= -k_B T \ln \mathcal{Z} \\ &= -k_B T \ln \mathcal{Z}_0 - k_B T \ln \langle e^{-\beta(H - H_0)} \rangle_0 \\ &= N \mathcal{F}_0 - k_B T \sum_{n=1}^{\infty} \frac{(-\beta)^n}{n!} \langle (H - H_0)^n \rangle_{0,c} \\ &= N(\mathcal{F}_0 + \mathcal{F}_1 + \mathcal{F}_2 + \cdots) . \end{aligned}$$

The first contribution $\mathcal{F}_0$ gives the contribution of N harmonic oscillators of frequency

$$\omega^2(p) = \Omega^2 + 4\phi \sin^2 \left[\frac{\pi p}{N} \right] ,$$

and its contribution to the free energy is

$$\mathcal{F}_0 = \frac{-k_B T}{2} \sum_{q=0}^{N-1} \ln \frac{2\pi k_B T}{\omega^2(p)} . \quad (19)$$

Introducing the parameters η, $\langle u^2 \rangle = \langle u_n^2 \rangle$, and $\langle v^2 \rangle = \langle u_n u_{n+1} \rangle$, the only difficulty in evaluating the variational free energy is the self-consistent substrate potential. Expanding the exponent in a series as follows (see appendix for the expression of $\langle u_k^{2p} \rangle$),

$$\begin{aligned} \langle e^{-a u_k} \rangle &= \left\langle \sum_p^{\infty} \frac{(-a)^p}{p!} u_k^p \right\rangle \\ &= \sum_p^{\infty} \frac{(-a)^{2p}}{(2p)!} \langle u_k^{2p} \rangle + \sum_p^{\infty} \frac{(-a)^{2p+1}}{(2p+1)!} \langle u_k^{2p+1} \rangle \\ &= \sum_p^{\infty} \frac{(-a)^{2p}}{(2p)!} \frac{(2p)!}{2^p p!} \langle u_k^2 \rangle^p + 0 = e^{a^2 \langle u^2 \rangle / 2} , \end{aligned} \quad (20)$$

we obtain an "effective" potential, which keeps the shape of the Morse potential, but with a minimum which is temperature dependent as shown in Fig. 9(a). The expression for the first-order correction for the free energy is then

$$\begin{aligned} \mathcal{F}_1 &= (K - \phi)(\langle u^2 \rangle - \langle v^2 \rangle) - \frac{\Omega^2}{2} \langle u^2 \rangle \\ &\quad + D(1 + e^{-2a\eta + 2a^2 \langle u^2 \rangle} - 2e^{-a\eta + (a^2/2)\langle u^2 \rangle}) . \end{aligned} \quad (21)$$

It can be shown [31] that the variational free energy gives an upper bound for the actual free energy

$$\mathcal{F} \leq \mathcal{F}_0 + \mathcal{F}_1 = \mathcal{F}_v . \quad (22)$$

Considering η, $\langle u^2 \rangle$, and $\langle v^2 \rangle$ as *variational* parameters, the conditions for $\mathcal{F}_v$ to be stationary are then equivalent to the system

$$\begin{aligned} \eta &= \frac{3a}{2} \langle u^2 \rangle , \\ \phi &= K , \\ \Omega^2 &= 2a^2 D e^{-2a\eta/3} . \end{aligned} \quad (23)$$

We can note that Ω^2 is temperature dependent but not ϕ, which means that the coupling constant is not renormalized in spite of the anharmonicity of the substrate potential. The phonon dispersion curve is just translated parallel to the frequency axis as the temperature changes. As

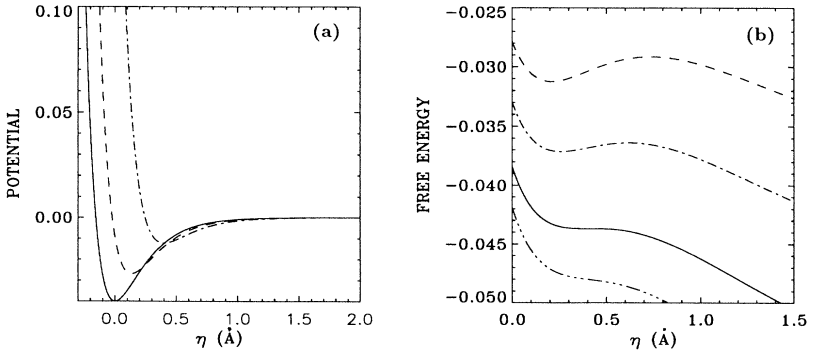

FIG. 9. (a) Substrate potential in the SCP approximation for a one-dimensional chain of Morse oscillators coupled by harmonic springs. The potential is plotted for the three following values of $\langle u^2 \rangle = 0$ (solid curve), 0.02 (dashed), 0.06 Å^2 (dash-dotted) (which corresponds to the three temperatures $T = 0$, 275, 411 K). (b) Free energy $\mathcal{F}_v$ vs η at different temperatures: $T = 350$ K (dashed curve), 380 K (dash-dotted), 411 K (solid), 430 K (dash-dot-dot-dot).

η is an increasing function of temperature, Ω^2 decreases with T which corresponds to the mode softening observed in the molecular-dynamics simulations.

Using the system (23), we can simplify the expression for the first-order correction of the free energy to obtain

$$\mathcal{F}_1 = D\left[1-(1+2a\eta/3)e^{-2a\eta/3}\right] . \tag{24}$$

Since $\langle u^2\rangle$ and η are related, the minimization of $\mathcal{F}_1$ amounts simply to solving the equation

$$\eta = \frac{3ak_BT}{2N}\sum_p \frac{1}{2a^2De^{-2a\eta/3}+4K\sin^2(\pi p/N)} . \tag{25}$$

In practice, Eq. (25) is solved by a simple bisection method and Fig. 9(b) shows the free energy $\mathcal{F}_v$ vs η at different temperatures. We see clearly that the self-consistent solution which corresponds to the metastable minimum of the dashed and dash-dotted curves, disappear at $T_c = 411$ K to give a strictly decreasing function of η. Over T_c the only minimum is obtained for an infinite value of η, which does not correspond to a self-consistent solution of the problem. Consequently T_c can be identified as the denaturation temperature given by the SCP. We can note that, at this temperature, a small well in the effective substrate potential on Fig. 9(a) persists, but it is not deep enough to support a bound state, i.e., a localized state.

Figure 10 presents $\mathcal{F}_v$ as function of T. While the SCP approximation is good at low temperature, as temperature rises, it becomes poor. This can be understood because, due to the even parity of the trial Hamiltonian H_0, the infinite number of odd powers in the Morse potential does not contribute to $\mathcal{F}_1$. A more accurate expression can be obtained by calculating the second-order correction $\mathcal{F}_2$ to the free energy. Using the expressions given in the appendix, we obtain the expression:

$$\mathcal{F}_2 = \frac{\langle (H-H_0)^2\rangle - \langle H-H_0\rangle^2}{-2Nk_BT}$$
$$= \frac{D^2}{2k_BT}e^{-(4/3)a\eta}\sum_l \left[(2e^{a^2\langle u_1u_l\rangle}-1)^2 - e^{4a^2\langle u_1u_l\rangle}+2a^4\langle u_1u_l\rangle^2\right] , \tag{26}$$

where

$$\langle u_1u_l\rangle = \frac{1}{N\beta}\sum_p \frac{\cos[(2\pi p/N)(l-1)]}{\Omega^2+4K\sin^2(\pi p/N)} .$$

Figure 10 shows that $\mathcal{F}_2$ significantly improves the agreement with the exact results up to about 300 K. However, the SCP calculation still fails for higher temperatures, emphasizing the fundamental role of the nonperturbative nonlinear effects in the denaturation process.

In the very-high-temperature regime, we can obtain a simple expression for the free energy because the whole system is on the plateau of the Morse potential, with an effective harmonic coupling constant K. Therefore, the model is equivalent to an harmonic chain, without substrate potential so that its free energy is simply

$$\mathcal{F}_{HT} = -\frac{k_BT}{2}\sum_{p=1}^{N-1}\ln\frac{\pi k_BT}{2K\sin^2(\pi p/N)} \tag{27}$$

and the specific heat per particle, in units of k_B, is equal to 1. Figures 2 and 10 show that, above the transition, this picture is indeed correct.

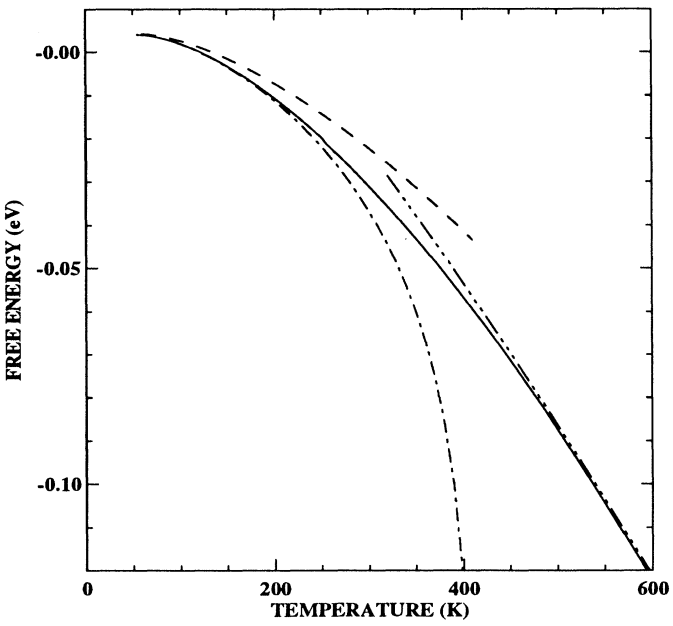

FIG. 10. Variation of the free energy vs temperature. The —— line corresponds to the exact free energy calculated with the transfer-integral method, the — — — line to the first-order SCP result, the —·—·— line to the second-order SCP, and the — · · · — line to the high-temperature harmonic approximation. Note that while the first-order SCP method is necessarily an upper bound to the exact free energy this is not a constraint for the second-order approximation.

V. CONCLUSION

The model that we have discussed can be considered as an extension of the Ising-like models for DNA melting, which includes a degree of freedom that describes the dynamics of the nucleotide motion. Therefore it can represent not only denaturation, but also precursor effects like fluctuational openings, which are a potential guide to the mechanism of denaturation. The numerical simulations have shown that, in spite of its simplicity with respect to the real DNA structure, the model provides a satisfactory qualitative description of DNA dynamics. In agreement with experimental results, we have found fluctuational openings and the formation of bubbles that grow and combine with each other to lead to a complete denaturation of the molecule.

Two complementary methods were used to study its statistical mechanics. The transfer integral has confirmed that the model should show a thermal denaturation and has pointed out that the lattice discreteness effects are large enough to change significantly the denaturation temperature. Since the denaturation occurs through a localization of the thermal energy which, in the limit where the model can be represented by a nonlinear Schrödinger equation can be viewed as the consequence of modula-

tional instability [9], one could expect that discreteness effects would increase this instability [32]. But discreteness also tends to prevent the growth of the denaturation bubbles by preventing an easy motion of their boundaries. The transfer-integral calculation shows that among these two contradictory effects of discreteness, the second one dominates. The SCP method has emphasized the dominant effects of the nonlinearity in a precursor regime near the transition. The use of the second-order correction to the free energy gives us a useful approach to obtaining analytical expressions for thermodynamic functions in the low- and intermediate-temperature range, but it fails in the vicinity of the denaturation. But the simple model that we have discussed here, although it goes far beyond the Ising models in its ability to describe the dynamics of the denaturation, is still not complete because it gives a transition which occurs at a rather high temperature (which could be related to our choice of parameters) and over too large a temperature region (which is a more fundamental limitation). This suggests that the model lacks sufficiently efficient mechanism for an energy localization. Work in this direction is currently in progress.

ACKNOWLEDGMENTS

The authors wish to acknowledge helpful and instructive discussions with S. Aubry, J.-L. Barrat, C. Reiss, and C. R. Willis. Two of us (T.D. and M.P.) are grateful for the hospitality of the Theoretical division and Center for Nonlinear Studies of Los Alamos National Laboratory. This work was performed with computing resources of the Advanced Computing Laboratory of Los Alamos National Laboratory. Part of the work has been supported by the CEC under Contract No. SC1-CT91-0705. Work at Los Alamos is under the auspices of the U.S. DOE.

APPENDIX: CALCULATION OF THE MEAN VALUES FOR THE SCP METHOD

(a) As H_0 is even, $\langle u_k^n u_l^p \rangle = 0$ if $(n+p)$ is odd. For calculating the even case, we introduce the matrix $\mathbf{M}$, with $M_{i,j} = (\Omega^2/2+\phi)\delta_{i,j} - (\phi/2)(\delta_{i,j+1}+\delta_{i,j-1})$.

$$\langle u_k^n u_l^p \rangle = \frac{\int \prod_i du_i u_k^n u_l^p \exp(-\beta \sum_{i,j} M_{i,j} u_i u_j)}{\int \prod_i du_i \exp -(\beta \sum_{i,j} M_{i,j} u_i u_j)}$$

$$= \frac{1}{\beta^{n+p} Z(\mathbf{0})} \left[\frac{\partial^{n+p}}{\partial h_k^n \partial h_l^p} \exp \left[-\beta \left[\sum_{i,j} M_{i,j} u_i u_j - \sum_i h_i u_i \right] \right] \right] \Bigg|_{\mathbf{h}=0} .$$

We introduce then the new variable $v_i = u_i - a_i$, where $\mathbf{a}$ is chosen so that the linear term of the quadratic form vanish. It gives $\mathbf{a} = \mathbf{M}^{-1}\mathbf{h}/2$. We obtain after long calculations [33]

$$\langle u_k^n u_l^p \rangle = \sum_{q=0}^{E(p/2)} \frac{n!p!}{(p-2q)!\{[n-(p-2q)]/2\}!q!} \frac{\langle u_k u_l \rangle^{p-2q} \langle u^2 \rangle^{(n-p)/2+2q}}{2^{(n-p)/2+2q}} . \tag{A1}$$

(b) Using again the same change of variable, we obtain

$$\langle e^{-a(u_k+u_l)} \rangle = \frac{\int \prod_i du_i e^{-a(u_k+u_l)} \exp \left[-\beta \sum_{i,j} M_{i,j} u_i u_j \right]}{\int \prod_i du_i \exp \left[-\beta \sum_{i,j} M_{i,j} u_i u_j \right]}$$

$$= \frac{1}{Z(\mathbf{0})} \int \prod_i du_i \exp \left[-\beta \left[\sum_{i,j} M_{i,j} u_i u_j - \sum_i h_i u_i \right] \right]$$

$$= e^{\beta^t \mathbf{h} \mathbf{M} \mathbf{h}/4} .$$

If $h_i = 0$, except $h_k = h_l = -a/\beta$, it reads as

$$\langle e^{-a(u_k+u_l)} \rangle = e^{a^2(\langle u^2 \rangle + \langle u_k u_l \rangle)} . \tag{A2}$$

The same calculation with $h_k = -2a/\beta$, gives

$$\langle e^{-a(2u_k+u_l)} \rangle = \exp[a^2(\tfrac{5}{2}\langle u^2 \rangle + 2\langle u_k u_l \rangle)] . \tag{A3}$$

(c) With the same trick, we have

$$\langle u_l^2 e^{-au_k} \rangle = \frac{\int \prod_i du_i u_l^2 e^{-au_k} \exp\left[-\beta \sum_{i,j} M_{i,j} u_i u_j\right]}{\int \prod_i du_i \exp\left[-\beta \sum_{i,j} M_{i,j} u_i u_j\right]}$$

$$= \frac{1}{\mathcal{Z}(0)} \int \prod_i du_i \frac{1}{\beta^2} \frac{\partial^2}{\partial h_l^2} \exp\left[-\beta\left[\sum_{i,j} M_{i,j} u_i u_j + \sum_i h_i u_i\right]\right]$$

$$= \frac{1}{\beta^2} \frac{\partial^2 e^{\beta\, {}^t\mathbf{h}\mathbf{M}\mathbf{h}/4}}{\partial h_l^2}$$

$$= \left[\frac{1}{\beta} \frac{\partial^2\, {}^t\mathbf{h}\mathbf{M}\mathbf{h}/4}{\partial h_l^2} + \left[\frac{\partial\, {}^t\mathbf{h}\mathbf{M}\mathbf{h}/4}{\partial h_l}\right]^2\right] e^{\beta\, {}^t\mathbf{h}\mathbf{M}\mathbf{h}/4} .$$

Therefore, with $h_i = 0$ except $h_k = -a/\beta$, it reads

$$\langle u_l^2 e^{-au_k} \rangle = [\langle u^2 \rangle + a^2 \langle u_k u_l \rangle^2] e^{(a^2/2)\langle u^2 \rangle} . \tag{A4}$$

---

*Permanent address: Laboratoire de Physique, ENS Lyon, 46 allée d'Italie, 69007 Lyon, France.

[1] M. Karplus and G. A. Petsko, Nature (London) **347**, 631 (1990); M. Karplus and J. A. McCammon, Sci. Am. **254**, 30 (1986).
[2] J. Ladik and J. Cizek, Int. J. Quantum Chem. **26**, 955 (1984).
[3] R. M. Wartell and A. S. Benight, Phys. Rep. **126**, 67 (1985).
[4] S. M. Englander *et al.*, Proc. Natl. Acad. Sci. (U.S.A.) **777**, 7222 (1980).
[5] V. Muto, A. C. Scott, and P. L. Christiansen, Phys. Lett. A **136**, 33 (1989).
[6] M. Techera, L. L. Daemen, and E. W. Prohofsky, Phys. Rev. A **42**, 5033 (1990).
[7] Y. Feng, R. D. Beger, X. Hua, and E. W. Prohofsky, Phys. Rev. A **40**, 4612 (1989).
[8] For a review see, G. Z. Zhou and C. T. Zhang, Phys. Scr. **43**, 347 (1991).
[9] M. Peyrard and A. Bishop, Phys. Rev. Lett. **62**, 2755 (1989).
[10] J. A. Mac Cammon and S. C. Harvey, *Dynamics of Proteins and Nucleic Acids* (Cambridge Univ. Press, Cambridge, 1988).
[11] D. J. Scalapino, M. Sears, and R. A. Ferrel, Phys. Rev. B **6**, 3409 (1972).
[12] J. A. Krumhansl and J. R. Schrieffer, Phys. Rev. B **11**, 3535 (1975).
[13] J. F. Currie, J. A. Krumhansl, A. R. Bishop, and S. E. Trullinger, Phys. Rev. B **22**, 47 (1980).
[14] P. M. Morse, Phys. Rev. **34**, 57 (1929).
[15] G. Dana Brabson, J. Chem. Educ. **50**, 397 (1973).
[16] J. L. Leroy, M. Kochoyan, T. Huynh-Dinh, and M. Gueron, Mol. Biol. **200**, 223 (1988).
[17] S. E. Trullinger and K. Sasaki, Physica D **28**, 181 (1988).
[18] T. Schneider and E. Stoll, Phys. Rev. B **22**, 5317 (1980).
[19] S. Nose, Mol. Phys. **52**, 255 (1984).
[20] S. Nose, J. Chem. Phys. **81**, 511 (1984).
[21] N. Theodorakopulos and M. Peyrard (unpublished).
[22] W. G. Hoover, Phys. Rev. A **31**, 1695 (1985).
[23] L. L. Van Zandt, Phys. Rev. A **40**, 6134 (1989); M. Techera, L. L. Daemen, and E. W. Prohofsky, *ibid.* **42**, 5033 (1990); L. L. Van Zandt, *ibid.* **42**, 5036 (1990); and references therein.
[24] Y. Gao, K. V. Devi Prasad, and E. W. Prohofsky, J. Chem. Phys. **80**, 6291 (1984).
[25] H. Teitelbaum and E. Englander, J. Mol. Biol. **92**, 55 (1975).
[26] E. W. Prohofsky *et al.*, Phys. Lett. **70A**, 492 (1979).
[27] T. Dauxois, M. Peyrard, and C. R. Willis, Physica D **57**, 267 (1992).
[28] J. L. Lebowitz, J. K. Percus, and L. Verlet, Phys. Rev. **153**, 250 (1967).
[29] N. Bocarra and G. Sarma, Physics (Long Island City) **1**, 219 (1965); J. R. Morris and R. J. Gooding, Phys. Rev. B **46**, 8733 (1992).
[30] Kubo, J. Phys. Soc. Jpn. **17**, 1100 (1962).
[31] R. P. Feynman, *Statistical Mechanics* (Benjamin, New York, 1972).
[32] Y. S. Kivshar and M. Peyrard, Phys. Rev. A **46**, 3198 (1992).
[33] T. Dauxois, Ph.D. thesis, Université de Bourgogne (unpublished).

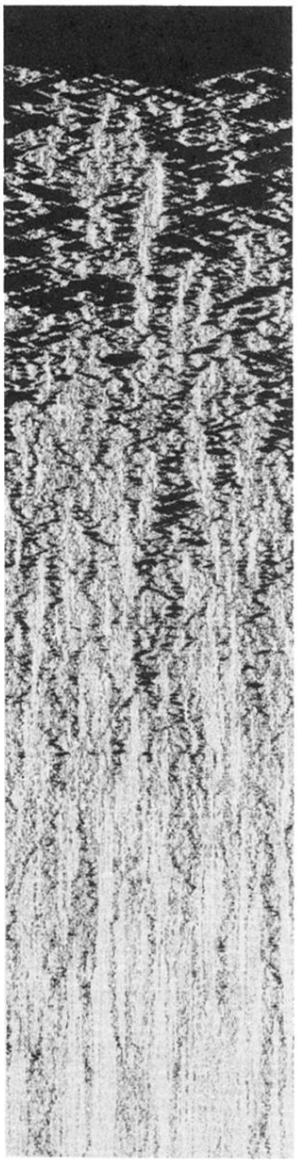

FIG. 3. Evolution of the stretching y along the DNA model during heating. The horizontal axis indicates the position along the 256 cells of the molecule and the vertical axis corresponds to the temperature (or time since t and temperature T are linearly related by the equation of the temperature ramp: $T=T_0+rt$). The temperature increases from 200 K (bottom) to 540 K (top). The grey scale goes from $y \leq 0$ Å (white) to $y \geq 2$ Å (black).

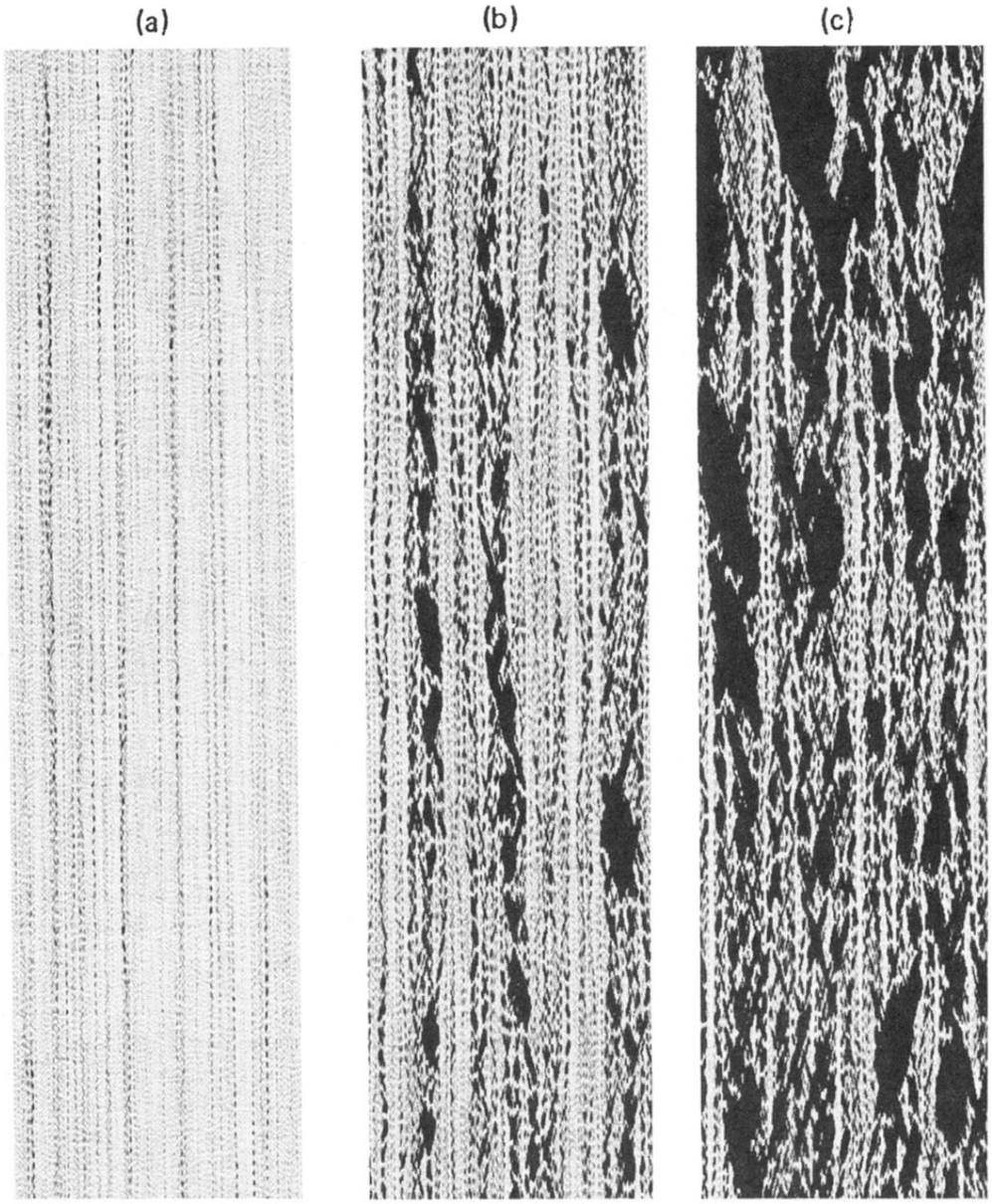

FIG. 4. Evolution vs time of the stretching for three equilibrium temperatures: (a) $T=150$ K, (b) $T=340$ K, (c) $T=450$ K. The grey scale goes from $y \leq -0.1$ Å (white) to $y \geq 1$ Å (black).